QUALIFICATION OF FREQUENCY RESPONSE FUNCTIONS USING THE RIGID-BODY RESPONSE

SAND--87-1634C

DE88 000745

David O. Smallwood
Jim P. Lauffer

Modal and Structural Mechanics Division
Sandia National Laboratories
Albuquerque, NM

ABSTRACT

The response of a structure at low frequencies with free boundary conditions is dominated by the rigid-body modes. The displacement shapes obtained from the low frequency values of the frequency response functions can be compared with ideal rigid-body motion to point out errors in the measurements. Insight is enhanced when the comparisons are made in the coordinate system of the measurements. Without this procedure intuition can rarely determine the proper rigid-body response at each measurement location. Typical errors identified are scaling errors, errors in location or direction, measurements with poor dynamic range and other instrumentaion problems. The procedure is particularly useful when the test object is multi-dimensional, has a complicated geometry, has measurements in other than rectangular coordinates, and where more than one rigid-body mode is excited. It is suggested that data qualification using this method would be a useful addition to most modal tests. A least squares approach, to determine the proper rigid-body response, is reviewed and several experimental examples are given.

NOMENCLATURE

a_i a vector denoting the sensitive axis in local coordinates of the ith measurement. For example, if the measurement was in the -z direction in the local coordinates (measurement coordinates) $a^T = [0\ 0\ -1]$ and if the measurement was in the +x direction then $a^T = [1\ 0\ 0]$. (3 x 1)

e an error vector, the difference between the measured rigid-body motion and an estimate of the rigid-body motion (N_m x 1)

e_{min} the residual error vector when the least squares estimate of p is used

i when used as a subscript or an argument, the measurement index

N_m the number of measurements

p a vector of modal participation factors for each of the rigid-body modes (6 x 1)

$\hat{p}$ a least squares estimate of p

T as a superscript, a matrix transpose

x,y,z rectangular coordinates

$\Phi_a(i)$ the analytical rigid-body mode shapes, in terms of the xyz coordinates of the ith measurement location (3 x 6)

Φ_b a matrix of rigid-body mode shapes expressed in terms of the measurement geometry (N_m x 6)

$\Phi_b(i)$ the ith row of Φ_b, the analytical rigid-body modes at the coordinates of the ith measurement (1 x 6)

Φ_r a vector of experimentally measured rigid-body motion (N_m x 1)

Λ_i a matrix to transform the global coordinates of the ith measurement point into the local measurement coordinates (3 x 3)

ξ^2 normalized square error

INTRODUCTION

The response of a freely suspended structure at low frequencies is a rigid-body response. The comparison of the measured responses with the ideal rigid-body response provides an easy way to detect errors in the measurements. Several authors[1,2] have made similar proposals for this use of the rigid-body modes. These authors suggested measuring one or more of the rigid-body modes. The resulting rigid-body mode shapes were then displayed in the global rectangular coordinates of the system for comparison with the analytical shapes. This paper will show that it is not necessary to directly measure the rigid-body modes; the information is contained in the values of the frequency response functions (FRFs) at low frequencies. An error mode shape is also derived which highlights the errors in the FRFs.

Another improvement is to keep the measurements and error measures in the local (measurement) coordinates. This will aid the user in several important ways. First the errors can be directly related to a particular measurement. This will be useful in efforts to isolate the source of an error. Second, by keeping the errors in the local coordinate system the requirements for a complete measurement set (i.e. measurements in all the x,y,z directions at each measurement location) are eliminated.

THEORY

Let

$$\Phi_r - \Phi_b\, p = e. \qquad (1)$$

The length of the vector Φ_r is N_m, the number of measurements. Typically, but not necessarily, three measurements are made at each location, resulting

DISCLAIMER

LEGIBILITY NOTICE

A major purpose of the Technical Information Center is to provide the broadest possible dissemination of information contained in DOE's Research and Development Reports to business, industry, the academic community, and federal, state, and local governments. Non-DOE originated information is also disseminated by the Technical Information Center to support ongoing DOE programs.

Although large portions of this report are not reproducible, it is being made available only in paper copy form to facilitate the availability of those parts of the document which are legible. Copies may be obtained from the National Technical Information Service. Authorized recipients may obtain a copy directly from the Department of Energy's Technical Information Center.

in measurements at $N_m/3$ geometric locations.

We will find a vector $\hat{p}$ which will minimize the normalized square error, ξ^2, where;

$$\xi^2 = e^T e/([\Phi_b \hat{p}]^T [\Phi_b \hat{p}]). \quad (2)$$

The least squares solution where the number of measurements, N_m, is greater than the number of participating rigid-body modes is given by

$$\hat{p} = [\Phi_b^T \Phi_b]^{-1} \Phi_b^T \Phi_r. \quad (3)$$

The residual error is given by

$$e_{min} = \Phi_r - \Phi_b \hat{p}. \quad (4)$$

The minimum normalized square error is given by

$$\xi^2 = e_{min}^T e_{min}/([\Phi_b \hat{p}]^T[\Phi_b \hat{p}]). \quad (5)$$

The product $\Phi_b \hat{p}$ is the best estimate of the rigid-body motion. The difference between this estimate and the measured rigid-body motion can tell us a great deal about the quality of individual measurements.

This information can be displayed in several ways. First the measured and the estimated rigid-body motions can be displayed as mode shapes. Any large differences will be apparent. Displays of the rigid-body shapes give an immediate feel for how closely the structure resembles a rigid-body at low frequencies. Second the error, e_{min}, can be displayed as a mode shape; this emphasizes the errors and makes them more apparent. We will refer to this as the error shape.

Displaying the error measures as mode shapes has the advantage of pointing to geometric areas of the structure with errors, and animating the mode shapes helps the eye pick out the errors. Mode shape displays in the global coordinate system have the disadvantage of making the one-to-one correspondence with the measurements difficult. The experimental motion, estimated motion, and error can also be displayed as functions of the measurement index. This makes the correspondence between errors and measurements clear, but can obscure the geometric relationships. Later examples will illustrate the advantages of using both methods.

To solve the above equations procedures for writing the matrices Φ_b and Φ_r must be developed. This will be done in the following sections.

DEVELOPMENT OF THE ANALYTICAL RIGID-BODY MODE SHAPES

The rigid-body mode shapes in the measurement coordinates can be generated from the geometry file in the following fashion. One row of the rigid-body mode shape matrix is given by,

$$\Phi_b(i) = a_i^T \Lambda_i \Phi_a(i) \quad (6)$$

where $\Phi_a(i)$ is the analytical reference mode shape given in terms of the measurement geometry by

$$\begin{array}{c} \\ x \\ y \\ z \end{array} \begin{array}{c} \begin{array}{cccccc} \text{trans} & \text{trans} & \text{trans} & \text{rot} & \text{rot} & \text{rot} \\ x & y & z & x & y & z \end{array} \\ \begin{bmatrix} 1 & 0 & 0 & 0 & z(i) & -y(i) \\ 0 & 1 & 0 & -z(i) & x(i) & 0 \\ 0 & 0 & 1 & y(i) & x(i) & 0 \end{bmatrix} \end{array} \quad (7)$$

Rows of the $\Phi_a(i)$ matrix represent contributions in the xyz directions respectively, and columns represent the rigid-body mode named above the matrix. The coordinates of the ith measurement location, in rectangular global coordinates are x(i), y(i), and z(i) respectively.

The transformation matrix ,Λ_i, transforms the rigid-body modes into the coordinate system of the measurements. We have implemented this transformation using Eulerian angles with the notation of Goldstein.[3] Many of our test items are frustums of cones and only the first two of the Eulerian rotations are needed.

The vector a_i is a three element vector used to select the sensitive coordinate axis of the transducer.

Note, the index i is a measurement index and is not a geometric location index. Typically, but not necessarily, three measurements (xyz) are located at the same location and will have the same Φ_a, and Λ_i matrices, but a different a_i vector.

DETERMINATION OF THE EXPERIMENTAL RIGID-BODY VECTOR, Φ_r

The accelerance frequency response functions (FRFs) (acceleration/force, with free boundary conditions) will follow a mass line at low frequencies (an example is shown in Fig. 4). The values of the FRFs over this region represent the inertia restraint of the rigid-body suspension modes. In a good experimental setup, the frequencies, where this mass like property is observed, is above any of the rigid-body suspension frequencies, but well below any flexural frequencies. A single value at one fixed frequency can be taken from each measurement FRF as an entry into the Φ_r vector; or because the measurements are frequently noisy at these frequencies, the real part of the FRFs can be averaged over a band of frequencies where the mass like behavior is observed. If the range is too close to an elastic mode of the structure, then the resulting shape will appear as a linear combination of the desired rigid-body shape and the first

elastic mode. If this is the case, then a different range can be selected and the rigid-body shape can be re-estimated. This method was used in this paper.

A second method is to measure one of the low frequency rigid-body suspension modes. This is what Crowley[1] recommends. The difficulty with this method is that these modes are frequently not available in the FRFs. When testing in the "free" condition every effort is made to force the rigid-body suspension frequencies as low as possible. If the experimental setup is good, these modes can lie below the measurement capability of the instrumentation system. For example, we typically will suspend a test item with the rigid-body modes below 2 Hz. The first flexural mode of interest might be as high as 150 Hz. The instrumentation system using piezoelectric accelerometers and charge amplifiers loses accuracy below 10 Hz. Also, the resolution of the FRFs, selected for analysis of the elastic modes, may be too large to resolve the rigid-body modes.

A third method is to use a curve fitting algorithm which includes residuals. All the low frequency elastic modes must be included, but not the rigid-body modes. The low frequency inertia restraint residual should be essentially the same value as the value from the first method, except the effects of nearby flexural modes will be compensated for correctly. This method should give the best estimates available for the inertia restraints. The disadvantage of the method is the estimates of the rigid-body modes for use as qualifiers for the data comes too late. We want to qualify the data before the curve fitting task. If the mass residuals are of critical importance for other needs this method can be used to refine the estimates, and the product $\Phi_b \hat{p}$ can be used to supply the best available estimates of rigid-body motion. Furusawa and Tominaga[2] made this suggestion.

ELIMINATION OF EXTREME DATA POINTS TO IMPROVE THE RIGID-BODY FIT

Data points which include errors beyond the usual random experimental errors can seriously affect the least squares rigid-body fit. The fit can be significantly improved by elimination of these measurements. This can be accomplished in either of two ways. The measurement can be removed from both Φ_b and Φ_r. This reduces the order of the matrices by one, for each measurement removed. Alternately, a weighting matrix can be used which will reduce the effect of the measurement to zero. We have used both methods. Using either method, the participation factors, $\hat{p}$, are recalculated after the measurements are eliminated and the normalized error, ξ, is recalculated. This error should drop sharply as the extreme measurements are eliminated. An indication that all the extreme values have been eliminated and only normal random errors remain is when the error ceases to drop sharply. The procedure is stopped at this point and the improved participation factors, $\hat{p}$, are used to recalculate the analytical rigid-body fit and error shape, which includes the extreme values.

IMPLEMENTATION OF TECHNIQUE AND EXAMPLES

The first example uses data from a test of a flat rectangular plate. The plate is the same plate used in another study.[4] Measurements were taken on a 5x7 grid resulting in 35 FRFs. Three figures are included to illustrate the data. Figure 1 is a plot of the normalized error as a function of the eliminated extreme measurements, Fig. 2 is a plot of the error plotted as a mode shape, and Fig. 3 is a plot of the error plotted as a function of measurement index. Clearly four measurements are in error; measurements 1, 30, and to a lesser extent 2 and 9. The rigid body fit was not significantly improved by removing any of the smaller errors.

Two modal surveys of axisymmetric structures were investigated to illustrate the advantage of using local coordinates for the calculations and displays. In both surveys, triaxial accelerometers were used to monitor the response. The triaxial blocks, on the exteriors of the structures, were aligned such that the x-axis of each triaxial accelerometer was mounted normal to the surface and the z-axis of the accelerometer lay in the plane formed by the x-axis of the accelerometer and axis of symmetry of the structure. Thus, the measurements at each point on the structure were in local rectangular coordinate systems. Because of limitations of the mode shape display software the rigid-body shapes estimated from the FRF data base were transformed into a global rectangular coordinate system for display. Displays which were functions of the measurement index were left in local coordinates.

To calculate the rigid-body shapes, the FRFs were reviewed to determine the range over which the FRFs followed a mass line, Fig. 4. The real parts of the individual FRFs were averaged over this range and entered into the corresponding location in the rigid-body shape, Φ_r. Averaging was performed because of the inherently low signal-to-noise ratio of the FRFs over the rigid-body response region of the FRFs. The shape was then transformed into global rectangular coordinates for display as a mode shape.

Measured rigid-body responses which deviated significantly from the from the analytical rigid-body least squares fit were given zero weighting and the participation factors for the analytical rigid-body shapes were re-estimated. This procedure is repeated until the differences between the measured and analytical shapes, for the non-zero weighted measurements, are uniform and are random indicating the elimination of all significant bias errors. These eliminated measurements correspond to measurements whose scale factor, direction, etc... may be in error.

A thin-walled right conic frustum, Fig. 5, was used for the next example. Figure 6 displays the analytical least squares shape (solid line) and the experimental shape (dashed line). While this plot gives one a qualitative feel as to the overall fit of the analytical to experimental shapes, individual bad data points do not necessarily

stand out because of the complicated geometry and because point(s) in error may not have a significant component in the viewing plane of the plot. A more meaningful representation is a plot of the analytical and experimental shapes as function of measurement index as in the plate example. For these plots, each response coordinate was assigned an integer abscissa value from one to the total number of response measurements. Ordinate values were the rigid-body shape entries for the corresponding response coordinates. Figure 7 displays the experimental (solid line) and analytical (circled line) shapes. Even more revealing, Fig. 8, is the error shape, the difference between the analytical and experimental shapes. The increasing error on the right hand side of the plot corresponds to the response of the first elastic mode of the frustum which is more apparent towards the large end of the structure. No significant bias errors are apparent.

The final test case studied was a modal survey of an earth penetrator. For this survey, three points on the structure were excited (1X, 1Z, 601X). They are illustrated in the undeformed geometry plot in Fig. 9. Fifty nine triaxial measurements and four points on the interior of the penetrator (801 through 804) were monitored for a total of 181 measurements. The nose of the penetrator appears deformed because no measurements were performed at the very tip. Figure 10 shows the analytical shape (solid line) plotted over the experimental shape (dashed line) for an input at 1Z. A geometric plot of the error shape is shown in Fig. 11. The error shape as a function of measurement index is shown in Fig. 12. Similar plots were generated for the other inputs, but are not included here. In each of the three types of plots, the measurements having the largest error (802X,Y,Z, measurement 171-173) are readily apparent; however, plots of the error shape as a function of the measurement index also indicated significant errors in the response at points 801Z, 803X,Y, and 804X,Y,Z. It was determined that the accelerometers at location 802 were grounded; 801Z and 804Z were mounted in the -Z direction instead of the +Z direction; and 803X,Y and 804X,Y were rotated a small angle from the correct axis during assembly.

CONCLUSIONS

The comparison of the rigid-body motion, determined from the mass line at the low frequencies of freely suspended structures, with a least squares analytical estimation of the rigid-body motion provides a quick and useful evaluation of the FRF data base. Using this technique, several common errors were detected, including; scaling errors, errors in location and direction and instrumentation problems. The approach is currently being used as part of our quality assurance procedure for freely suspended modal tests. Similar procedures are being used for motion controlled vibration tests.

REFERENCES

1. Crowley, Brown, and Rocklin, "Uses of Rigid Body Calculations in Test," Proc. of the 4th IMAC, pp 487-491, Feb. 1986.
2. Furusawa and Tominaga, "Rigid Body Mode Enhancement and Rotational DOF Estimation for Experimental Modal Analysis," Proc. of the 4th IMAC, pp 1149-1155, Feb. 1986.
3. Goldstein, H., **Classical Mechanics**, Addison-Wesley, Reading Mass., 1959, pp 107-109.
4. Smallwood, D. O., and Gregory, D. L., "A Rectangular Plate Is Proposed as an IES Modal Test Structure", Proc. of the 4th IMAC, pp 1246-1255, Feb. 1986.

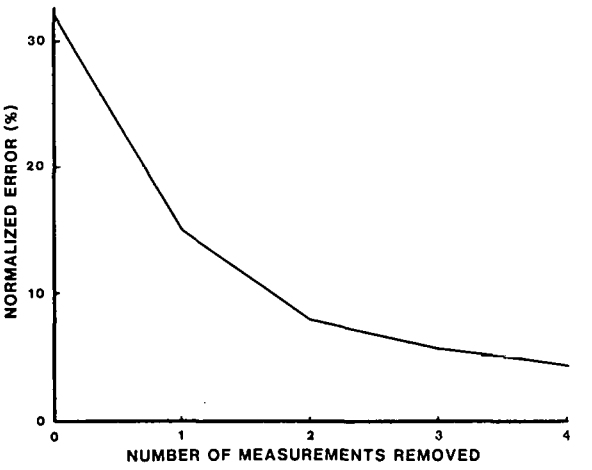

Fig. 1 Normalized Error in the Rigid-Body Modes of a Plate as a Function of the Number of Removed Measurements

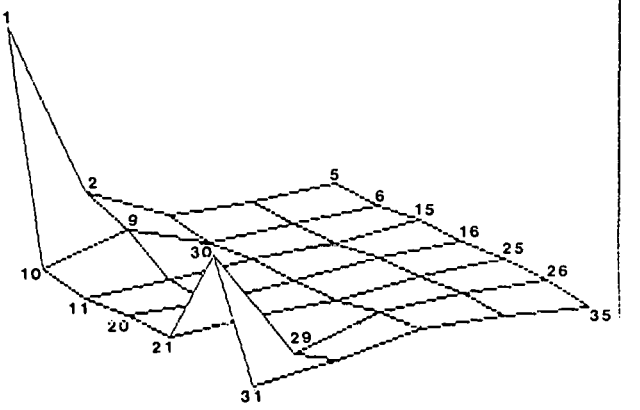

Fig. 2 Plate Error Mode Shape

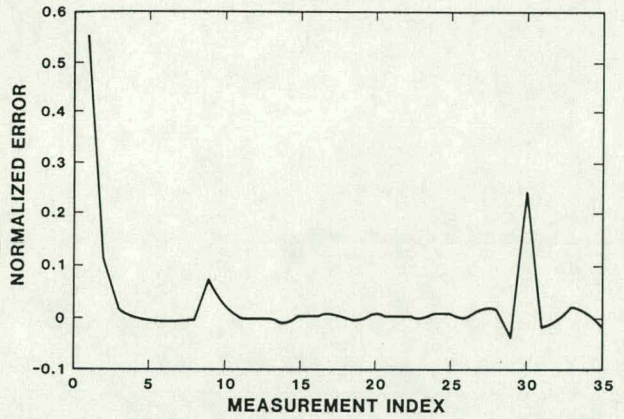

Fig. 3 Plate Error as a Function of Measurement Location

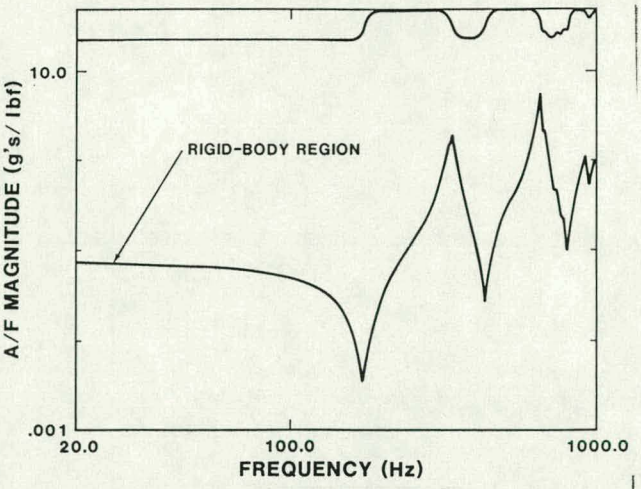

Fig. 4 Driving Point FRF

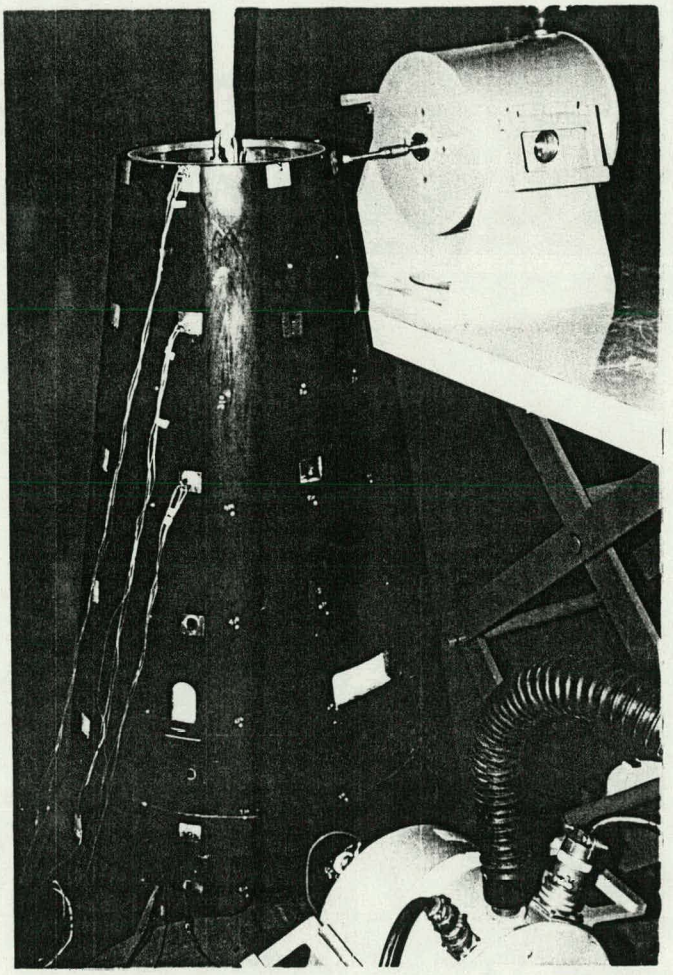

Fig. 5 Test Configuration for the Modal Survey of a Fustrum

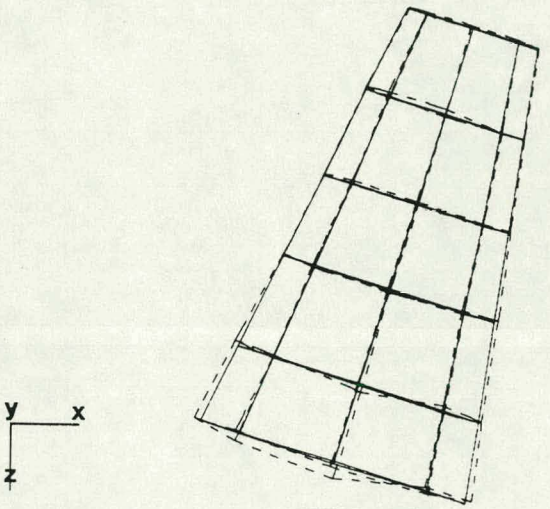

Fig. 6 Experimental and Fitted Rigid-Body Mode Shapes When Driving at the Top

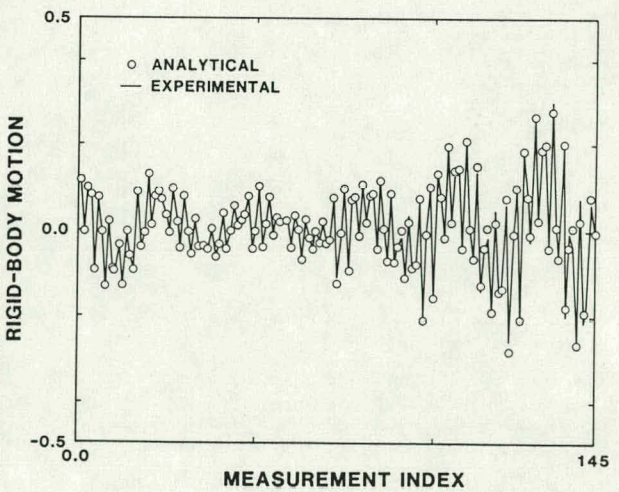

Fig. 7 Experimental and Fitted Shapes When Driving at the Base

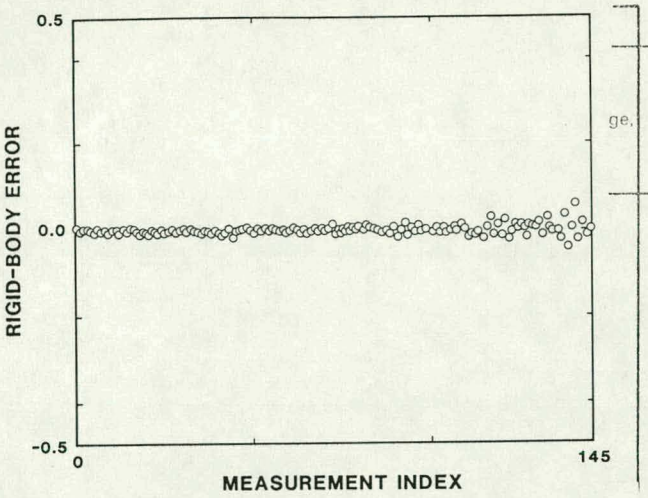

Fig. 8 Rigid-Body Error Shape When Driving at the Base

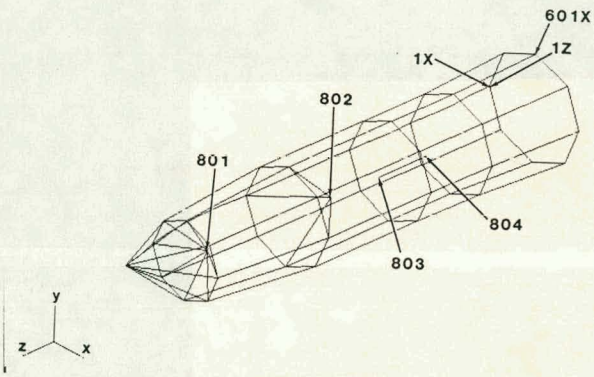

Fig. 9 Undeformed Geometry of an Earth Penetrator

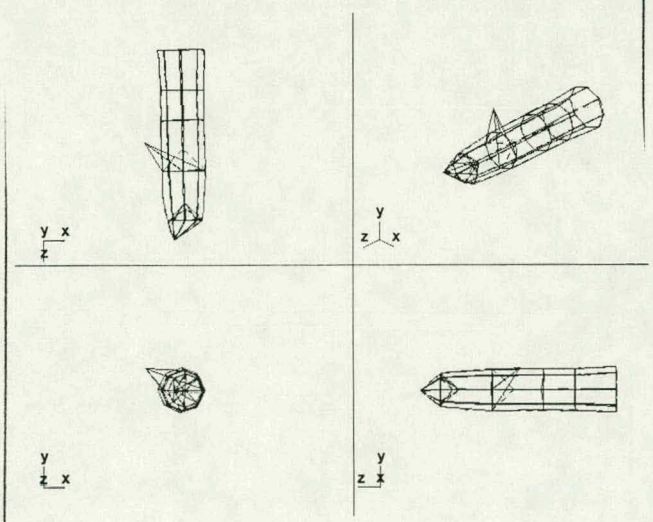

Fig. 10 Experimental and Fitted Rigid-Body Mode Shapes for an Input at 1Z

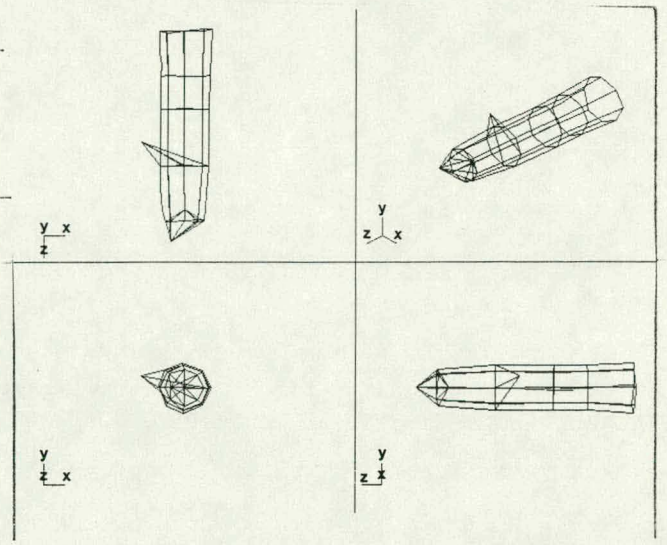

Fig. 11 Error Mode Shape for an Input at 1Z

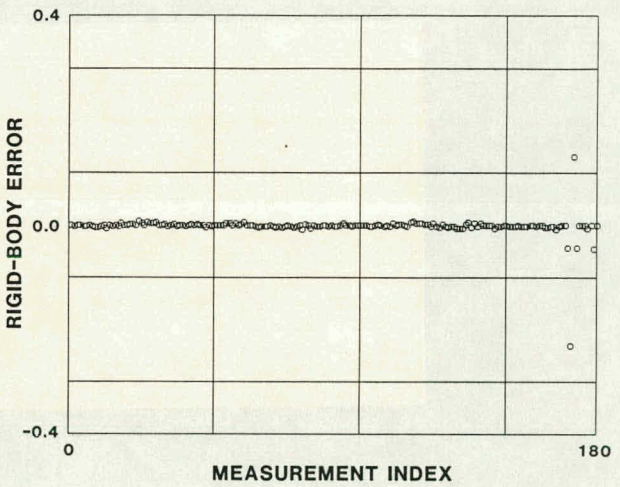

Fig. 12 Rigid-Body Error Shape When for an Input at 1Z